Subseasonal Zonal Oscillation of the Western Pacific Subtropical High during Early Summer

Weina GUAN, Xuejuan REN*, Wei SHANG, and Haibo HU

China Meteorological Administration–Nanjing University Joint Laboratory for Climate Prediction Studies, School of Atmospheric Sciences, Nanjing University, Nanjing 210023

(Received April 11, 2018; in final form June 19, 2018)

ABSTRACT

This study examines the features and dynamical processes of subseasonal zonal oscillation of the western Pacific subtropical high (WPSH) during early summer, by performing a multivariate empirical orthogonal function (MV-EOF) analysis on daily winds and a diagnosis on potential vorticity (PV) at 500 hPa for the period 1979–2016. The first MV-EOF mode is characterized by an anticyclonic anomaly occupying southeastern China to subtropical western North Pacific regions. It has a period of 10–25 days and represents zonal shift of the WPSH. When the WPSH stretches more westward, the South Asian high (SAH) extends more eastward. Above-normal precipitation is observed over the Yangtze–Huaihe River (YHR) basin. Suppressed convection with anomalous descending motion is located over the subtropical western North Pacific. The relative zonal movement of the SAH and the WPSH helps to establish an anomalous local vertical circulation of ascending motion with upper-level divergence over the YHR basin and descending motion with upper-level convergence over the subtropical western Pacific. The above local vertical circulation provides a dynamic condition for persistent rainfall over the YHR basin. An enhanced southwest flow over the WPSH's western edge transports more moisture to eastern China, providing a necessary water vapor condition for the persistent rainfall over the YHR basin. A potential vorticity diagnosis reveals that anomalous diabatic heating is a main source for PV generation. The anomalous cooling over the subtropical western Pacific produces a local negative PV center at 500 hPa. The anomalous heating over the YHR basin generates a local positive PV center. The above south–north dipolar structure of PV anomaly along with the climatological southerly flow leads to northward advection of negative PV. These two processes are conducive to the WPSH's westward extension. The vertical advection process is unfavorable to the westward extension but contributes to the eastward retreat of the WPSH.

Key words: western Pacific subtropical high, subseasonal timescale, diabatic heating, potential vorticity

Citation: Guan, W. N., X. J. Ren, W. Shang, et al., 2018: Subseasonal zonal oscillation of the western Pacific subtropical high during early summer. *J. Meteor. Res.*, **32**(5), 768–780, doi: 10.1007/s13351-018-8061-2.

1. Introduction

The western Pacific subtropical high (WPSH) is a large-scale anticyclonic circulation in the mid–lower troposphere. Its major body is located over the western Pacific during summer. The WPSH is usually represented by the 5880-gpm isoline in the 500-hPa geopotential height fields (Tao and Chen, 1987). The location and intensity of the WPSH determine the confluence of the warm and humid air from the oceanic region and the cold and dry air from mid to high latitudes. Thus, the WPSH has profound influences on the weather and climate over the East Asian monsoon region (Wu et al., 1999; Lu, 2001; Lu and Dong, 2001; Mao et al., 2003; Wen et al., 2003; Liu et al., 2004; Ding and Chan, 2005; Zhou et al., 2009; Wang et al., 2011; Hong and Ren, 2013; Yang et al., 2014; He et al., 2015).

The WPSH exhibits variations on the subseasonal timescale (Huang et al., 2003). Especially, the western edge of the WPSH exhibits a process of migration first westward then eastward on a 10–30-day period during early summer. This zonal movement of the WPSH plays a crucial role in the development of severe droughts or floods over East Asia (Wen and Shi, 2006; Wang et al., 2009; Mao et al., 2010; Ren et al., 2013; Chen and Zhai, 2015; Qian and Shi, 2017). Thus, investigations of the

Supported by the National Natural Science foundation of China (41621005, 41675067, and 41330420).

*Corresponding author: renxuej@nju.edu.cn.

WPSH's subseasonal zonal movement have attracted much attention since the 1960s (Huang, 1963; Tao and Zhu, 1964). The present study focuses on the features and dynamical processes of the WPSH's subseasonal zonal movement.

When the WPSH extends westward (retreats eastward) on the subseasonal timescale, an anomalous high center is seen over Southeast Asia and its coastal region. Above-normal water vapor is transported towards eastern Asia (Mao et al., 2010; Ren et al., 2013; Yang et al., 2014). The movement of the WPSH coordinates with other circulations. For example, when the WPSH extends westward, the South Asian high (SAH) at the upper level stretches eastward. The subseasonal relative zonal motion of the WPSH and the SAH contributes to the rainfall anomalies over eastern China during summer (Liu et al., 2006; Ren et al., 2007; Chen and Zhai, 2016).

Some investigations indicated that the subseasonal eastward stretch of the SAH at the upper level is in favor of the westward extension of the WPSH (Ren et al., 2007; Chen and Zhai, 2016). Other studies showed that the subseasonal zonal oscillation of the WPSH is associated with a quasi-biweekly oscillation propagating northwestward from the tropical to the subtropical western Pacific at mid–lower levels (Hsu and Weng, 2001; Jia and Yang, 2013; Chen et al., 2015; Li et al., 2015). Especially, the WPSH's westward extension is accompanied by the northwestward migrating anticyclonic phase of the quasi-biweekly oscillation. Thus, the latter may be responsible for the former (Yang et al., 2010; Li et al., 2015). We speculate that both the migration of the SAH in the upper troposphere and the quasi-biweekly oscillation in the mid–lower troposphere are responsible for the subseasonal westward extension of WPSH. The related evolution features and dynamical processes need to be investigated in a coherent way. This study intends to reveal the dynamical mechanisms for the WPSH's zonal oscillation through performing a diagnosis on potential vorticity (PV).

It is noted that a northward jump of the WPSH occurs over the western North Pacific in mid July (Tao and Chen, 1987; Lu, 2001; Ding and Chan, 2005; Yang et al., 2014). The variations of atmospheric circulation and rainfall over East Asia show differences before and after mid July (Ding and Chan, 2005). During early summer, the 10–30-day zonal oscillation of the WPSH is more dominant than that during the late summer. Thus, we focus on early summer (1 June–20 July) in this paper.

In summary, this study focuses on the following two aspects: 1) the features of the zonal oscillation of the WPSH at 500 hPa on the subseasonal timescale, and the associated large-scale circulation (especially the SAH); and 2) the dynamical processes contributing to the subseasonal zonal movement of the WPSH. The remainder of this paper is organized as follows. Data and methods are introduced in Section 2. Section 3 investigates the feature of the WPSH's subseasonal zonal oscillation during early summer, and its connection with large-scale circulation and rainfall anomalies. Section 4 analyzes the related dynamical processes. A summary is given in Section 5.

2. Data and analysis methods

2.1 *Data*

The 0.5° × 0.5° gridded observations of daily precipitation covering global land areas developed by the US Climate Prediction Center (CPC) are used in this study. This gridded precipitation product came from rain gauge observations over global land areas (Chen et al., 2008). Daily mean outgoing longwave radiation (OLR) on a 2.5° × 2.5° spatial resolution from the National Oceanic and Atmospheric Administration (NOAA) is used (Liebmann and Smith, 1996). The daily atmospheric elements are from the ECMWF interim reanalysis (ERA-Interim; Dee et al., 2011) at a resolution of 0.75° × 0.75°. All datasets cover the period 1979–2016.

2.2 *Methods*

The diabatic heating Q_1 is calculated according to the method introduced by Yanai et al. (1973) and Yanai and Tomita (1998):

$$Q_1 = \frac{\partial T}{\partial t} + \boldsymbol{V}_\mathrm{h}\cdot\nabla_\mathrm{h}T + \omega\left(\frac{\partial T}{\partial p} - \frac{RT}{c_p p}\right), \tag{1}$$

where T, R, and c_p are the air temperature, the gas constant for dry air, and the specific heat of dry air at constant pressure, respectively. $\boldsymbol{V}_\mathrm{h} = (u, v)$ is the horizontal wind, ω is the vertical velocity in pressure (p) coordinates, and ∇_h is the horizontal gradient operator. Vertical integration of Q_1 is from the tropopause pressure (p_t) to the surface pressure (p_s) as follows,

$$\langle Q_1\rangle = \frac{c_p}{g}\int_{p_\mathrm{t}}^{p_\mathrm{s}} Q_1 \mathrm{d}p, \tag{2}$$

where g is the gravitational acceleration and p_t is set to be 100 hPa.

The anticyclonic circulation corresponds to low PV values. In terms of isobaric PV, if ignoring the friction term, the local tendency of PV is expressed as (Zhang and Ling, 2012; Ren et al., 2015)

$$\frac{\partial \mathrm{PV}}{\partial t} = -\underbrace{\left(u\frac{\partial \mathrm{PV}}{\partial x} + v\frac{\partial \mathrm{PV}}{\partial y}\right)}_{\text{part-}h} - \underbrace{\omega\frac{\partial \mathrm{PV}}{\partial p}}_{\text{part-}w} - \underbrace{g(f+\zeta)\frac{\partial Q_1}{\partial p}}_{\text{PVG}} - g\left(\zeta_x\frac{\partial Q_1}{\partial x} + \zeta_y\frac{\partial Q_1}{\partial y}\right), \quad (3)$$

where ζ_x is the zonal relative vorticity and ζ_y the meridional one. The term $-(u\frac{\partial \mathrm{PV}}{\partial x} + v\frac{\partial \mathrm{PV}}{\partial y})$ is PV advection via horizontal winds (part-h). The term $-(\omega\frac{\partial \mathrm{PV}}{\partial p})$ is PV vertical advection (part-w). The term $-g(f+\zeta)\frac{\partial Q_1}{\partial p}$ is non-uniform distribution of Q_1 in the vertical direction. It is a PV generation (PVG) term. The last term in Eq. (3) is also a PV generation term via horizontal non-uniform distribution of Q_1. The last term is not considered due to its much smaller value than the others. Thus, PV generation results mainly from the vertical gradient of Q_1.

By using the method introduced by Zhang and Ling (2012) and Ren et al. (2015), a variable is divided into its time mean (denoted by an overbar) and subseasonal (denoted by a prime) and non-subseasonal components. The subseasonal anomalies of local PV changes ($\partial \mathrm{PV}'/\partial t$) are decided by the following processes:

$$\left(\frac{\partial \mathrm{PV}'}{\partial t}\right)_{\text{part-}h} = -\left(\bar{u}\frac{\partial \mathrm{PV}'}{\partial x} + \bar{v}\frac{\partial \mathrm{PV}'}{\partial y}\right) - \left(u'\frac{\partial \overline{\mathrm{PV}}}{\partial x} + v'\frac{\partial \overline{\mathrm{PV}}}{\partial y}\right) + \text{residue-}h, \quad (4)$$

$$\left(\frac{\partial \mathrm{PV}'}{\partial t}\right)_{\text{part-}w} = -\bar{\omega}\frac{\partial \mathrm{PV}'}{\partial p} - \omega'\frac{\partial \overline{\mathrm{PV}}}{\partial p} + \text{residue-}w, \quad (5)$$

$$\left(\frac{\partial \mathrm{PV}'}{\partial t}\right)_{\mathrm{PVG}} = -g(f+\bar{\zeta})\frac{\partial Q_1'}{\partial p} - g\zeta'\frac{\partial \overline{Q_1}}{\partial p} + \text{residue-}Q, \quad (6)$$

where residue-h, residue-w, and residue-Q are the residual terms. They express nonlinear interactions between subseasonal and non-subseasonal timescales. The terms of residue-w and residue-Q contribute about 10% to their individual $\partial \mathrm{PV}'/\partial t$ over East Asia and its coastal region. The term of residue-h is slightly higher than 10%. This study focuses on the subseasonal timescale. Thus, the three residual terms are ignored. Main contributors to Eqs. (4)–(6) are: the horizontal advection of subseasonal PV anomaly $[-(\bar{u}\,\partial \mathrm{PV}'/\partial x + \bar{v}\,\partial \mathrm{PV}'/\partial y)]$ in Eq. (4), the vertical advection via ω' and the vertical distribution of climatological PV $[-\omega'(\partial \overline{\mathrm{PV}}/\partial p)]$ in Eq. (5), and the vertical distribution of the subseasonal Q_1 anomaly, i.e., $[-g(f+\bar{\zeta})\partial Q_1'/\partial p]$ in Eq. (6), respectively.

The procedure to obtain the subseasonal anomalies of every variable is as follows (Ren et al., 2015). Firstly, we use a five-day running mean to remove very high frequency fluctuations in the daily data. Then, we discard the daily climatology; and lastly, the interannual timescale is eliminated via deducting seasonal anomaly. A multivariate empirical orthogonal function (MV-EOF) analysis is used to obtain the spatiotemporal features of zonal oscillation of the WPSH on the subseasonal timescale. The MV-EOF analysis is performed on normalized subseasonal anomalies in horizontal winds (u and v) at 500 hPa over the region (0°–45°N, 110°–150°E) for the period of early summer (1 June–20 July) from 1979 to 2016 (total 1900 days). In comparison with a regular EOF analysis, the MV-EOF is more suitable to capture the spatial distributions of several selected variables and the co-variability relationship among these variables. Time-lagged regressions of the subseasonal variables on the standardized first principal components of MV-EOF (PC1) are calculated. Day 0 means simultaneous regression. A negative lag day (a positive lag day) is performed by shifting backward (forward) the number of the leading (lag) days.

3. Subseasonal zonal oscillation of the WPSH and accompanied anomalies in large-scale circulation

3.1 *Basic features*

Figure 1 depicts the climatological early summer (1 June–20 July) fields of geopotential height and horizontal wind at 500 and 200 hPa (Z500, Z200), vertical wind fields at 400 hPa (w400), and precipitation during early summer. The WPSH, which is represented by 5880-gpm isoline (hereafter 5880-line) at 500 hPa, is zonally elongated over the western Pacific. Its ridge axis is along 22°N. The 200-hPa SAH's body section is represented by the 12,520 gpm contour (12,520-line). The middle and eastern part of the SAH's main body is located over the region from northern India Peninsula to western Pacific between 20° and 30°N. The westerly flow is located over the poleward side of the SAH and the WPSH. The western edge of the WPSH is occupied by southerlies. Strong ascending motion is seen over the south and north flanks of the WPSH. Abundant rainfall is observed over South Asia, East Asia, and the continents near the equator.

Figure 2a shows the spatial pattern of the first MV-EOF mode (MV-EOF1), which accounts for 11.6% of the total subseasonal variance. Although the percentage

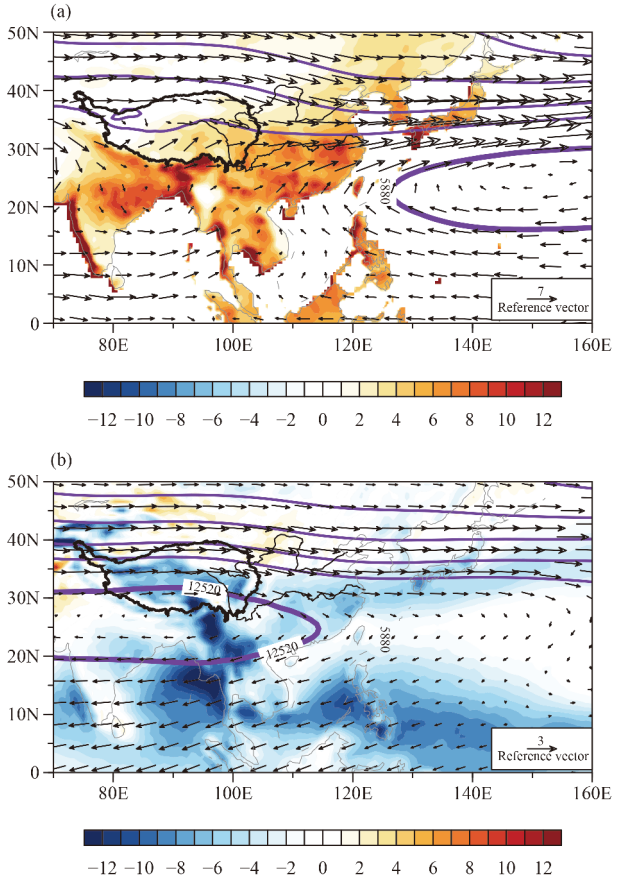

Fig. 1. Climatological early summer (1 June–20 July) fields of (a) geopotential height at 500 hPa (Z500, blue contour of 60-gpm intervals), horizontal winds at 500 hPa (vector, m s^{-1}), and rainfall (shaded, mm day^{-1}); and (b) geopotential height at 200 hPa (Z200, blue contour of 120-gpm intervals), horizontal winds at 200 hPa (vector, m s^{-1}), and vertical velocity ω at 400 hPa (w400, shaded, 0.01 Pa s^{-1}).

variance for the first MV-EOF1 mode is small, it is statistically distinguishable from the other modes according to the rule of North et al. (1982). The pattern of MV-EOF1 is characterized by an anticyclonic anomaly occupying the WPSH's western part. The PC1 shows a periodicity of 10–25 days (Fig. 2b). This periodicity is a dominant timescale of subseasonal zonal movement of the WPSH during early summer (Zhang and Yu, 1992; Wen et al., 2003; Ren et al., 2013; Yang et al., 2014). Figure 2c displays the normalized time series of the PC1 for summer 1995. The WPSH's westward and eastward events are picked according to the normalized time series of the PC1. A westward (eastward) event is selected when the normalized PC1 is $\geqslant$ ($\leqslant$) 1.0 (–1.0) in at least three consecutive days. During the early summers of 1979–2016, 41 westward events and 45 eastward events are identified with the above criteria.

The leading/lagged composites of the 5880-line at 500 hPa for the westward and eastward events are plotted in Fig. 3. The leading/lags show a range from –12 to 12 days with an interval of 3 days. The zonal oscillation of the WPSH is the dominant feature of the MV-EOF1. For the leading composite of the westward events, the west point of the 5880-line at day –12 is located near 132°E (Fig. 3a). It stretches westward slightly at day –9. The western edge passes southern Taiwan with an accelerated speed and finally reaches the westernmost location at day 0 (Fig. 3a). The WPSH stays for three days at its westernmost position. After that, the WPSH begins to withdraw eastward. It is over the western Pacific on day +9 (Fig. 3b). The leading/lagged composites of the 5880-line shown in Figs. 3c, d also present zonal oscillation but with the zonal migration first eastward (Fig. 3c) and then westward (Fig. 3d).

The simultaneous composites of subseasonal circulation and related features for the westward and eastward events of the WPSH are shown in Fig. 4. The 5880-line advances more westward for the westward events than the eastward events (Figs. 4a, d). For the westward events, an anomalous anticyclonic circulation is centered over the western part of the WPSH from southeastern China to the subtropical western North Pacific, while a cyclonic one exists poleward of the anomalous anticyclone (Fig. 4a). Meanwhile, negative OLR anomalies and anomalous ascending motion are observed over the Yangtze–Huaihe River (YHR) basin in China, accompanied by enhanced precipitation, and a large area of suppressed convection with positive OLR anomalies and anomalous descending motion is located over the subtropical western North Pacific, indicating locally reduced precipitation there (Fig. 4b). For the westward events, the anomalous anticyclone over the western part of the WPSH transports more water vapor to the YHR basin in China, resulting in anomalous moisture convergence over there and moisture divergence over the subtropical western North Pacific (Fig. 4c). The simultaneous fields of anomalies in OLR, vertical motion, precipitation, and water vapor transport for the eastward events are almost opposite to the patterns for the westward ones (Figs. 4d, e, f).

3.2 *Relative zonal shift of the SAH and the WPSH*

The time-lagged regression of Z500 and Z200 anomalies, as well as w400 anomaly onto the normalized PC1 are plotted in Fig. 5, superimposed on time-lagged compositions of 5880-line and 12,520-line for the westward events. We first analyze the evolution at 500 hPa (left panels in Fig. 5). At the WPSH's early stage of westward extension (during days –9 to –6), a center with weak positive Z500 anomaly and anomalous descending

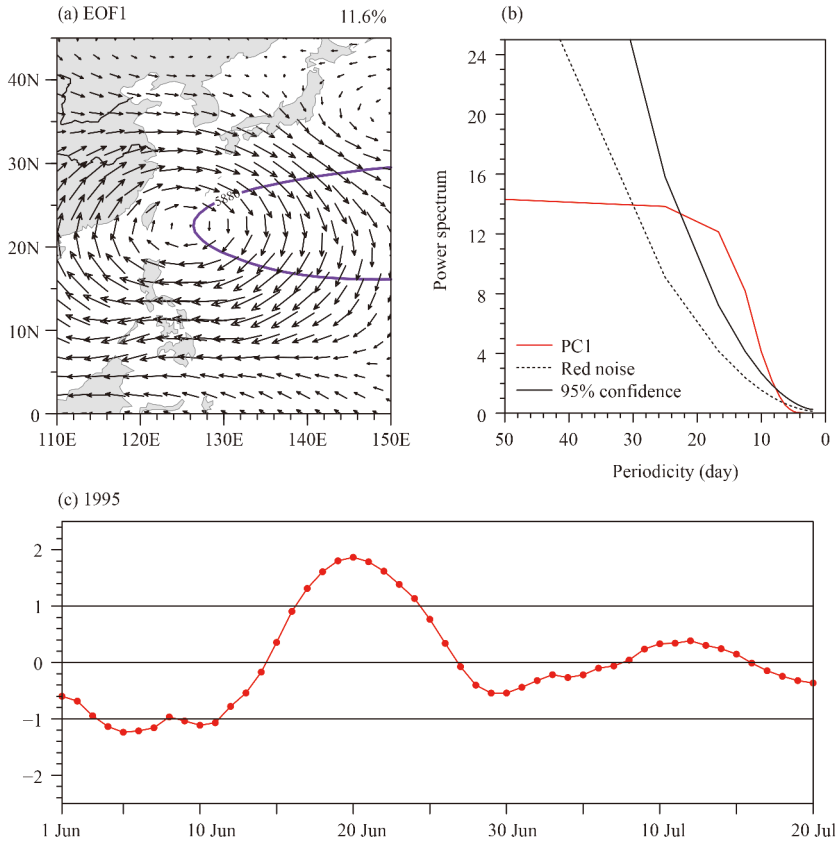

Fig. 2. (a) Spatial pattern of MV-EOF1 on normalized subseasonal anomalies in horizontal winds (u and v) at 500 hPa during early summer of 1979–2016. (b) Averaged mean power spectra (red line) of the principal component of MV-EOF1. (c) Time series of daily PC1 for the summer of 1995 (red line). The blue line in (a) is the climatological 5880-line. The black dashed line in (b) is the red noise spectrum and the black solid line in (b) is the spectrum of 95% confidence level.

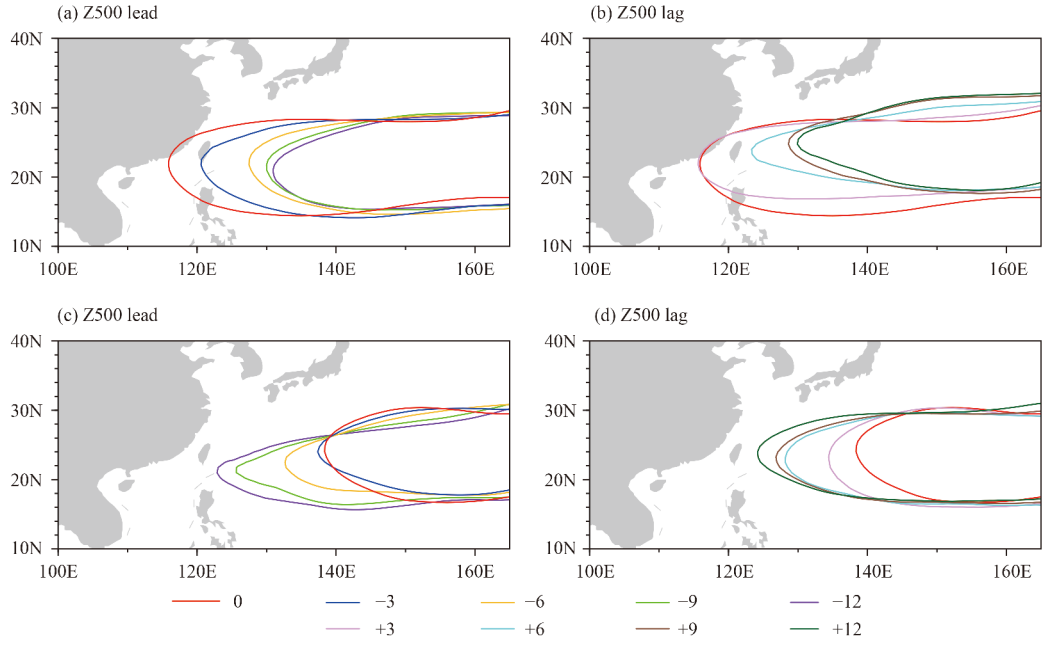

Fig. 3. Composites of the 5880-line at 500 hPa for (a, d) westward events and (b, c) eastward events from (a, c) day –12 to (b, d) day +12 with intervals of 3 days.

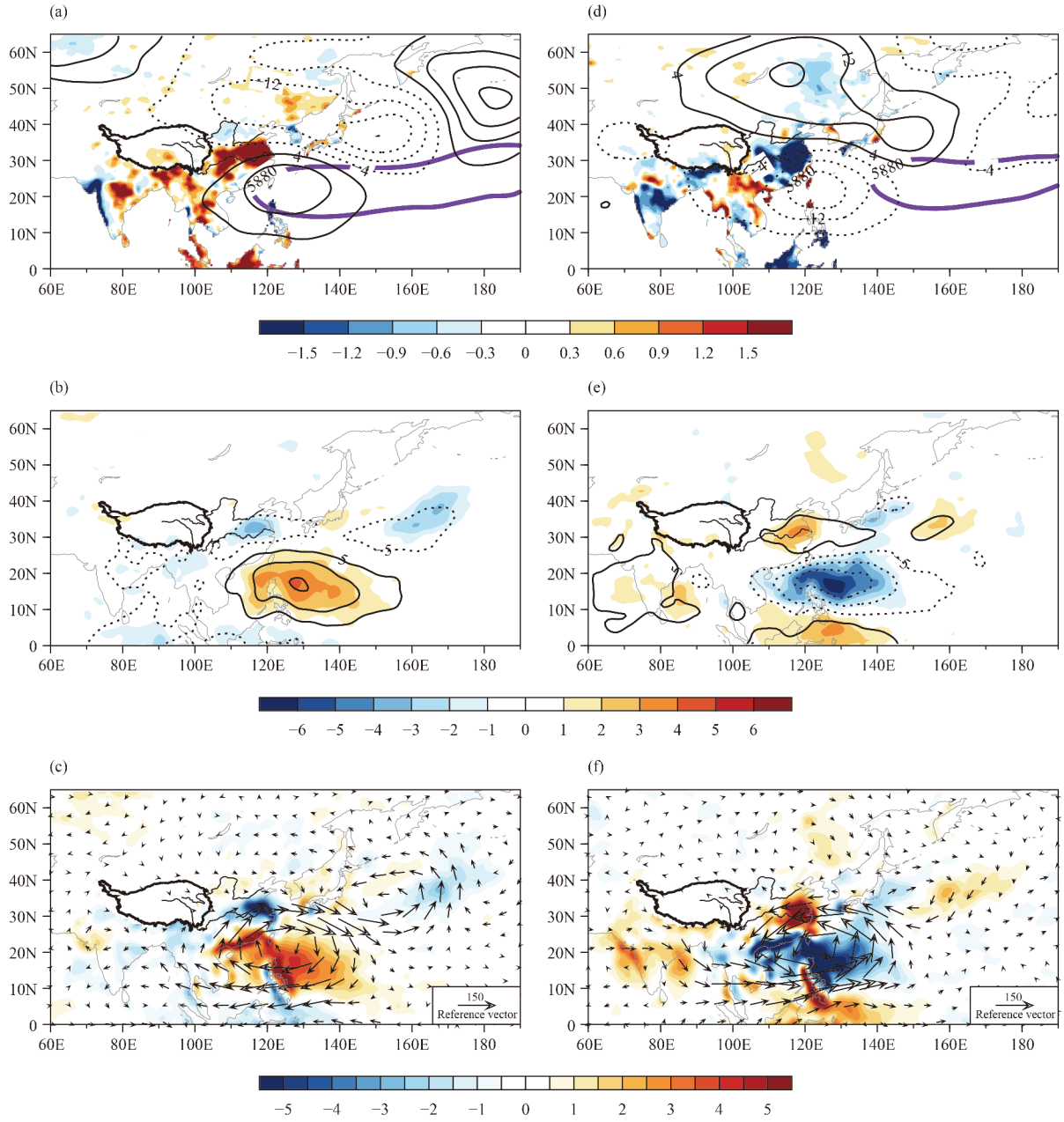

Fig. 4. Simultaneous composites of subseasonal circulation for (a–c) westward and (d–f) eastward events. (a, d) Subseasonal anomalies in Z500 (black contour, gpm) and precipitation (shaded, mm day^{-1}) superimposed on the composite climatological 5880-line (thick blue contour). (b, e) Subseasonal anomalies in w400 (black contour, 0.01 Pa s^{-1}) and OLR (shaded, W m^{-2}). (c, f) Subseasonal anomalies in integrated water vapor transport (IVT, vector, kg m^{-1} s^{-1}) and its divergence (shaded, 10^{-5} kg m^{-2} s^{-1}). Zero contours are omitted in all figures.

motion are seen over the subtropical western Pacific to the east of 120°E. Accompanied by the robustly westward extension of the WPSH, above positive anomalous center propagates northwestward toward East Asian coastal waters with an increasing amplitude, and reaches eastern Asia and its coastal waters at day 0. After day 0, the above positive Z500 anomaly begins to weaken. Meanwhile, the WPSH begins to retreat eastward. During the process, anomalous ascending motion is established gradually over the YHR basin from days –9 to –3. It reaches its peak at day 0, corresponding to the locally above-normal precipitation shown in Fig. 4a.

In the upper troposphere, the SAH shows eastward extension during days –9 to 0 and then westward retreat after day 0 (right panels in Fig. 5). Accompanied by the eastward stretch of the SAH, a negative Z200 anomalous center with anomalous convergence is seen over the subtropical western North Pacific. Meanwhile, a positive

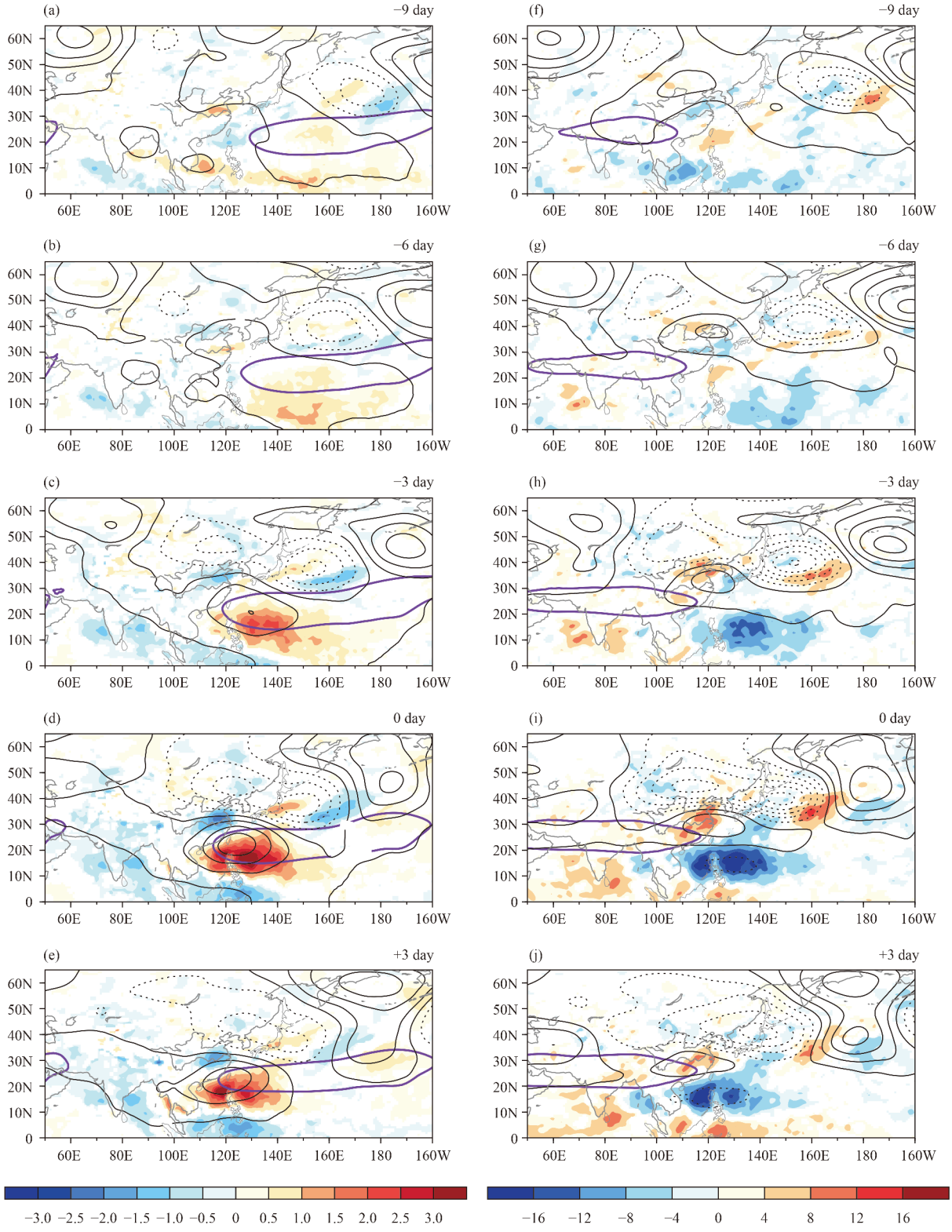

Fig. 5. Regressed fields of (a–e) Z500 (black contour at intervals of 4 gpm) and w400 (shaded, 0.01 Pa s^{-1}) anomalies; and (f–j) Z200 anomalies (black contour at intervals of 5 gpm) and divergence of horizontal winds at 200 hPa (shaded, 10^{-7} s^{-1}) onto the normalized PC1 for days –9, –6, –3, 0, and +3 for westward events. The composite 5880-line at 500 hPa in (a–e) and the composite 12,520-line at 200 hPa in (f–j) for the westward events are plotted as thick blue contours. The shading denotes significant area at the 95% confidence level for w400 in (a–e) and divergence of horizontal winds at 200 hPa in (f–j).

Z200 anomalous center with anomalous divergence is observed over eastern China. At both 500 and 200 hPa, a wave train is seen across Eurasian continent north of 35°N. It is especially clear at 200 hPa. A positive–negative–positive pattern with centers over West Siberian Plain, west of Lake Baikal and southeast of Lake Baikal is established at day –9, and then moves to southeast from day –9 to 0. At day 0, the low center of the wave train is located poleward of the YHR region.

Figure 6a displays the longitude–time section (averaged over 10°–25°N) of regressed anomalies in Z500 and OLR onto the normalized PC1. The above anticyclonic circulation with suppressed convective activity is firstly seen over the subtropical western Pacific at 150°E around day –9. It then propagates westward and reaches its peak at day 0 and day +1 between 120° and 130°E. After day +3, it fades away. Accompanied by the above signal, the western ridge points of the WPSH, which are denoted by the blue dots in Fig. 6a, move westward gradually and then retreat eastward after day +2. Figure 6b is the longitude–time section (averaged over 25°–35°N) of regressed anomalies in Z200, OLR, and precipitation. Accompanied by the eastward extension of the SAH's eastern ridge point (blue dot in Fig. 6b), positive Z200 anomalies are established over East China and its coastal waters. Meanwhile, persistent rainfall is seen over the YHR basin.

3.3 *Vertical structure*

Figure 7 shows latitude–height sections of regressed anomalies in geopotential height, wind fields of v and ω, and divergence of horizontal wind averaged over 110°–125°E. During days –6 to –4, a low–high–low pattern is established in the upper troposphere. Ascending motion over the YHR basin and weak descending motion over subtropical western North Pacific are observed at mid–lower levels (Fig. 7a). Meanwhile, weak divergence is seen south of 40°N (Fig. 7d). During days –3 and –1, the anomalous local vertical circulation of mid-level intensified ascending motion with upper-level divergence over the YHR basin, and mid-level descending motion with upper-level convergence over subtropical western North Pacific, is established well (Figs. 7b, e). During days 0 to +2, this anomalous local vertical anomalous circulation reaches its mature stage. Above analysis indicates that the eastward extension of SAH is favorable for the establishment of the vertical meridional circulation during the westward extension of the WPSH, which provides a necessary dynamical condition for persistent rainfall over the YHR basin.

4. Dynamical processes for the subseasonal zonal shift of WPSH

Figure 8 plots the longitude–time section (averaged over 10°–25°N) and latitude–time section (averaged over 110°–135°E) of regressed anomalies in Z500 and PV at 500 hPa (PV500). The propagating characteristics of PV500 are indeed similar to those of Z500. A negative PV500 anomaly is corresponding to a positive Z500 anomaly. In the following, we show the three dynamical processes responsible for the WPSH's subseasonal zonal shift by performing the PV diagnostic analysis according to Eqs. (4) –(6).

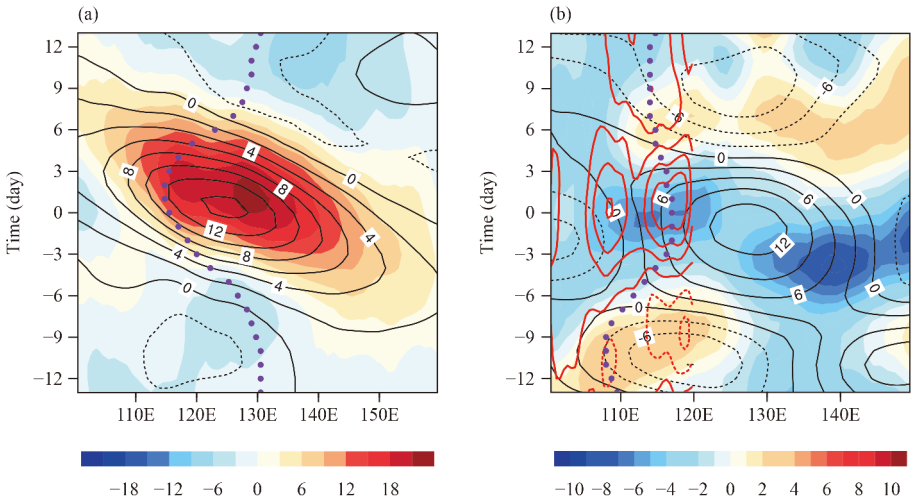

Fig. 6. Longitude–time sections of regressed subseasonal anomalies in (a) Z500 (contour, gpm) and OLR (shaded, W m^{-2}) averaged over 10°–25°N; and (b) Z200 (contour, gpm), OLR (shaded, W m^{-2}), and precipitation (red contour with interval of 0.5 mm day^{-1}), averaged over 25°–35°N. Western ridge points of the WPSH in (a) and eastern ridge points of the SAH in (b) are denoted by blue dots.

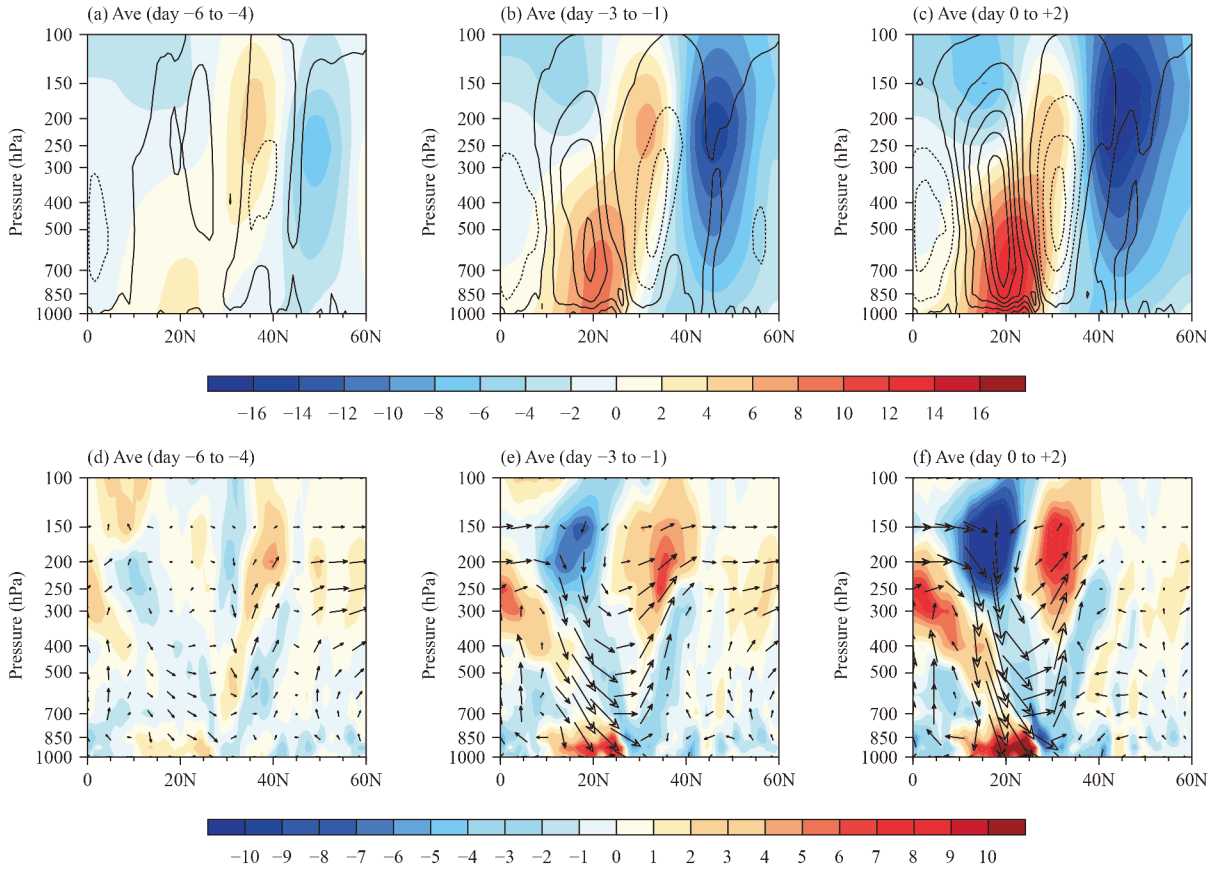

Fig. 7. Latitude–height sections (averaged over 110°–125°E) of regressed subseasonal anomalies in (a–c) geopotential height (shaded, gpm) and vertical velocity ω (black contour at intervals of 0.004 Pa s^{-1}); and (d–f) wind fields (vector; v, m s^{-1}; ω, –0.01 Pa s^{-1}) and divergence of horizontal wind (shaded, 10^{-7}s^{-1}), averaged between days (a, d) –6 and –4, (b, e) –3 and –1, and (c, f) 0 and +2.

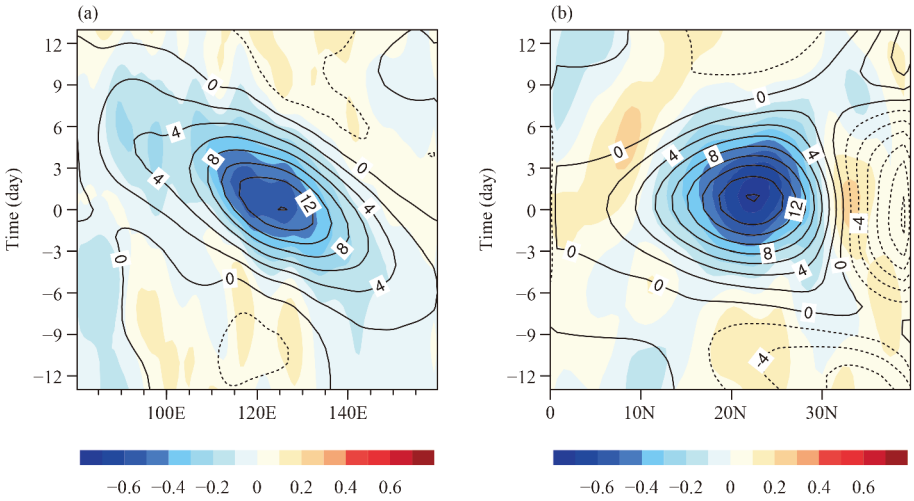

Fig. 8. Longitude–time sections of regressed subseasonal anomalies in (a) PV500 (shaded, 0.1 PVU) superimposed on Z500 anomalies (contour, gpm) averaged over 10°–25°N. (b) Same as (a) but for latitude–time section averaged over 110°–135°E.

Figure 9 shows regression fields of subseasonal anomalies of PVG, part-w, and part-h onto the normalized PC1 averaged from day –3 to +3. The PVG anomalies at 500 hPa are decided mostly by the PV generation term $[-g(f+\bar{\zeta})\partial Q_1'/\partial p]$. The PVG term and $-\partial Q'/\partial p$ are alike in the spatial pattern and propagation features. The non-uniform rainfall patterns over the subtropical western North Pacific and eastern China can induce anomalous

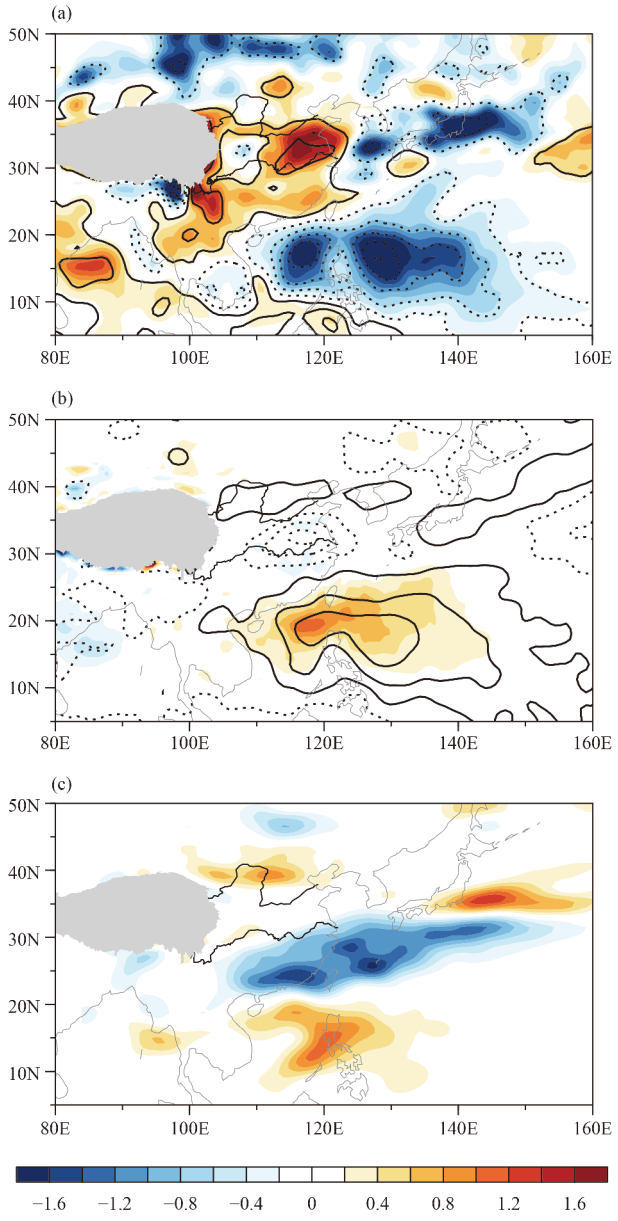

Fig. 9. Regressed subseasonal anomalies of (a) PVG term (shaded, 0.01 PVU day^{-1}) and vertical gradient of diabatic heating ($-\partial Q'/\partial p$) (black contour at intervals of 10^{-3} K day^{-1} hPa^{-1}), (b) part-w term (shaded, 0.01 PVU day^{-1}) and w500 (black contour at intervals of 0.01 Pa s^{-1}), and (c) part-h term (shaded, 0.01 PVU day^{-1}) onto the normalized PC1, averaged between days –3 and +3 (with zero contour omitted).

distributions in diabatic heating. During the period of days –3 to +3, the rainfall anomalies over the East Asian region reach the peak. Negative Rainfall anomalies over the subtropical western North Pacific leads to negative $-\partial Q'/\partial p$. Negative $-\partial Q'/\partial p$ induces negative $-g(f+\bar{\zeta})\,\partial Q_1'/\partial p$ and then contributes to negative PV anomaly. Meanwhile, positive rainfall anomaly over eastern China and to the south of the Tibetan Plateau generates positive PV locally (Fig. 9a). The term part-w is caused mostly by $-\omega'(\partial\overline{\mathrm{PV}}/\partial p)$. It is mainly determined by subseasonal anomalies of vertical velocity (ω') at mid–high levels. This is because the climatological PV decreases from high to low level. Thus, the $-\partial\overline{\mathrm{PV}}/\partial p$ term is always positive at 500 hPa over the subtropical East Asia to western Pacific regions. Anomalous descending motion carries high PV value from high level to lower level, causing positive PV anomalies at 500 hPa over the subtropical western North Pacific (Fig. 9b). Because the patterns of Q' and ω' are alike, the feature of the PVG term in Fig. 9a bears close resemblance to that of the part-w term in Fig. 9b.

It can be noted that the negative PV anomaly generated by $-\partial Q'/\partial p$ is only located over the subtropical western North Pacific south of 20°N (Fig. 9a). Thus, it can only contribute to the anomalous anticyclone at 500 hPa over oceanic region. In the observation (left panel in Fig. 5), the western part of the 500-hPa anomalous anticyclone as well as the 5880-line is located over southeastern China. Other dynamical process should be responsible for the landing of the 500-hPa anomalous anticyclone and the WPSH's 5880-line during days –3 to +3. That is the horizontal advection process. The term part-h is mainly determined by climatological horizontal winds and horizontal gradient of subseasonal PV anomaly in Eq. (4) $[-(\bar{u}\ \partial \mathrm{PV}'/\partial x + \bar{v}\ \partial \mathrm{PV}'/\partial y)]$. Because of the north positive–south negative PV pattern in Fig. 9a and climatological southerly over the western part of the WPSH, negative PV anomalies is transported northward from the subtropical western North Pacific to southern China and its coastal waters (Fig. 9c). Therefore, the term part-h is responsible for the landing of the 500 hPa anomalous anticyclone and thus the westernmost and northernmost position of WPSH during days –3 to +3.

To show the evolution of above three processes, the latitude–time sections of the three terms (PVG, part-w, and part-h) are plotted in Fig. 10, averaged over 110°–135°E . The vertical gradient of diabatic heating ($-\partial Q'/\partial p$) is also plotted in Fig. 10a. It bears close resemblance with the PVG term. During days –6 to +6, a south negative–north positive pattern of PVG term is significantly seen in Fig. 10a. The negative diabatic anomalies (decreased rainfall and anomalous descending motion) over the subtropical western North Pacific contribute to the increasing of negative PV locally during days –3 to 0 through the PVG term. The part-w term's position overlaps mostly with that of PV500 anomalies in Fig. 10b. The anomalous descending motion over the subtropical western North Pacific increases positive PV locally through the part-w term. Thus, it is unfavorable to

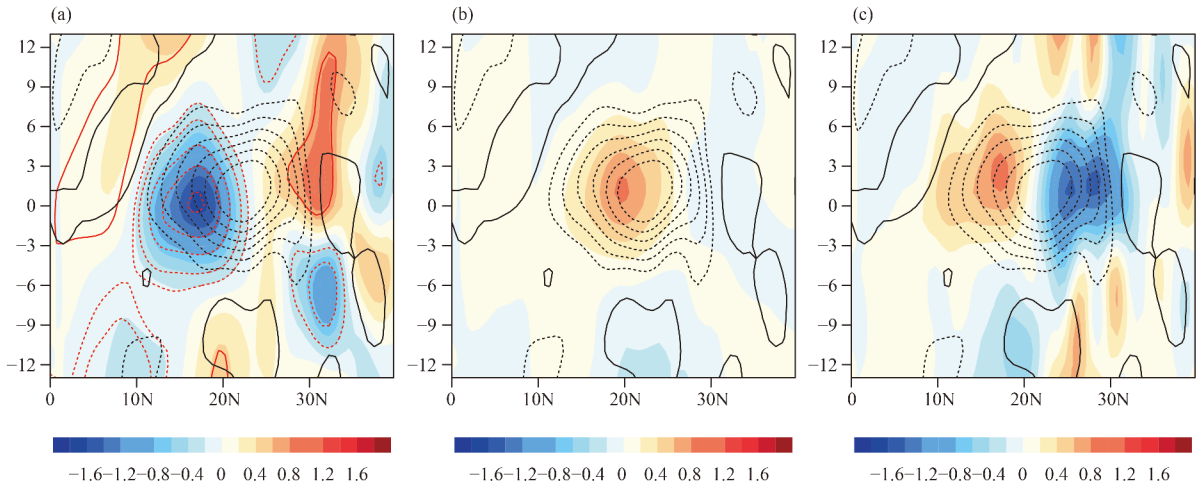

Fig. 10. Latitude–time sections of regressed subseasonal anomalies averaged over 110°–135°E of (a) PVG term (shaded, 0.01 PVU day^{-1}) and $-\partial Q'/\partial p$ (red contour at intervals of 10^{-3} K day^{-1} hPa^{-1}) at 500 hPa, (b) part-w term (shaded, 0.01 PVU day^{-1}), and (c) part-h term (shaded, 0.01 PVU day^{-1}). The black contours in (a–c) denote regressed subseasonal anomalies of PV500 at intervals of 0.01 PVU. The y-axis is time (day).

the westward extension but favors the eastward retreat of the WPSH. The part-h term causes negative PV500 (positive Z500) anomaly north of 20°N during days –6 to +6. As mentioned above, it favors westward and northward extension of the WPSH to the land region.

5. Summary

This study investigates features of zonal oscillation of the WPSH at 500 hPa during early summer on the subseasonal timescale, and the related three dynamical processes responsible for the zonal movement of the WPSH. The MV-EOF analysis is conducted by using daily horizontal winds at 500 hPa over the region (0°–45°N, 110°–150°E) for the period of 1 June–20 July from 1979 to 2016. The first MV-EOF mode shows that an anticyclone circulation occupies over the western part of the WPSH, reflecting zonal oscillation of the WPSH. The PC1 time series have a periodicity of 10–25 days. When the WPSH reaches its westernmost position, a strong anomalous high at Z500 fields is sustained over southeastern China and the subtropical western North Pacific. Meanwhile, above-normal precipitation occurs over the YHR basin and below-normal precipitation occurs over the subtropical western North Pacific. For the eastward events, the WPSH is located more eastward with opposite circulation and rainfall patterns compared with the westward events.

The WPSH's westward shift is accompanied by the eastward stretch of the SAH. The relative zonal movement of the SAH and the WPSH results in an anomalously local vertical circulation of ascending motion in the troposphere with upper-level divergence over the YHR basin, and descending motion with upper-level convergence over the subtropical western Pacific. This pattern is a dynamic condition for persistent rainfall over the YHR basin. The enhanced southwestly over the WPSH's western edge transports more moisture towards the YHR basin, providing necessary water vapor condition for persistent rainfall over there.

The PV500 anomalies on the subseasonal timescale over the East Asian region are mainly decided by the subseasonal anomalies in PV generation term, and the vertical and horizontal advection terms. The subseasonal anomaly of PV generation is mainly due to vertical nonuniformity of diabatic heating. The vertical advection term is determined by anomalous vertical motion. The horizontal advection term mainly depends on climatology horizontal winds and the horizontal gradient of PV anomaly.

The northwestward propagation of the suppressed convection (negative Q') over the subtropical western North Pacific induces a negative PV anomaly locally, via the diabatic heating feedback process. Meanwhile, the positive rainfall anomaly over the YHR basin generates a positive PV anomaly locally. Because of the above meridional gradient of PV anomalies and the climatological southerly flow over the western edge of the WPSH, the horizontal advection process transports the negative PV anomaly northward. These two processes (PVG and part-h) favor the subseasonal westward extension of the WPSH. The vertical advection process induces a positive PV anomaly over the subtropical western North Pacific, being unfavorable to the westward extension but

contributing to the eastward retreat of the WPSH.

REFERENCES

Chen, J. P., Z. P. Wen, R. G. Wu, et al., 2015: Influences of northward propagating 25–90 day and quasi-biweekly oscillations on eastern China summer rainfall. *Climate Dyn.*, **45**, 105–124, doi: 10.1007/s00382-014-2334-y.

Chen, M. Y., W. Shi, P. P. Xie, et al., 2008: Assessing objective techniques for gauge-based analyses of global daily precipitation. *J. Geophys. Res.*, **113**, D04110, doi: 10.1029/2007JD009132.

Chen, Y., and P. M. Zhai, 2015: Synoptic-scale precursors of the East Asia/Pacific teleconnection pattern responsible for persistent extreme precipitation in the Yangtze River Valley. *Quart. J. Roy. Meteor. Soc.*, **141**, 1389–1403, doi: 10.1002/qj.2448.

Chen, Y., and P. M. Zhai, 2016: Mechanisms for concurrent low-latitude circulation anomalies responsible for persistent extreme precipitation in the Yangtze River Valley. *Climate Dyn.*, **47**, 989–1006, doi: 10.1007/s00382-015-2885-6.

Dee, D. P., S. M. Uppala, A. J. Simmons, et al., 2011: The ERA-Interim reanalysis: Configuration and performance of the data assimilation system. *Quart. J. Roy. Meteor. Soc.*, **137**, 553–597, doi: 10.1002/qj.828.

Ding, Y. H., and J. C. L. Chan, 2005: The East Asian summer monsoon: An overview. *Meteor. Atmos. Phys.*, **89**, 117–142, doi: 10.1007/s00703-005-0125-z.

He, C., T. J. Zhou, and B. Wu, 2015: The key oceanic regions responsible for the interannual variability of the western North Pacific subtropical high and associated mechanisms. *J. Meteor. Res.*, **29**, 562–575, doi: 10.1007/s13351-015-5037-3.

Hong, W., and X. Ren, 2013: Persistent heavy rainfall over south china during May–August: Subseasonal anomalies of circulation and sea surface temperature. *Acta Meteor. Sinica*, **27**, 769–787, doi: 10.1007/s13351-013-0607-8.

Hsu, H. H., and C. H. Weng, 2001: Northwestward propagation of the intraseasonal oscillation in the western North Pacific during the boreal summer: Structure and mechanism. *J. Climate*, **14**, 3834–3850, doi: 10.1175/1520-0442(2001)014<3834:NPOTIO>2.0.CO;2.

Huang, R. H., L. T. Zhou, and W. Chen, 2003: The progresses of recent studies on the variabilities of the East Asian monsoon and their causes. *Adv. Atmos. Sci.*, **20**, 55–69, doi: 10.1007/BF03342050.

Huang, S. S., 1963: A study of the longitudinal movement and its forecasting of subtropical anticyclones. *Acta Meteor. Sinica*, **33**, 320–332, doi: 10.11676/qxxb1963.030. (in Chinese)

Jia, X. L., and S. Yang, 2013: Impact of the quasi-biweekly oscillation over the western North Pacific on East Asian subtropical monsoon during early summer. *J. Geophys. Res.*, **118**, 4421–4434, doi: 10.1002/jgrd.50422.

Li, C. H., T. Li, A. L. Lin, et al., 2015: Relationship between summer rainfall anomalies and sub-seasonal oscillations in South China. *Climate Dyn.*, **44**, 423–439, doi: 10.1007/s00382-014-2172-y.

Liebmann, B., and C. A. Smith, 1996: Description of a complete (interpolated) outgoing longwave radiation dataset. *Bull. Amer. Meteor. Soc.*, **77**, 1275–1277.

Liu, H. Z., S. R. Zhao, C. G. Zhao, et al., 2006: Weather abnormal and evolutions of western Pacific subtropical high and South Asian high in summer of 2003. *Plateau Meteor.*, **25**, 169–178, doi: 10.3321/j.issn:1000-0534.2006.02.001. (in Chinese)

Liu, Y. M., G. X. Wu, and R. C. Ren, 2004: Relationship between the subtropical anticyclone and diabatic heating. *J. Climate*, **17**, 682–698, doi: 10.1175/1520-0442(2004)017<0682:RBTSAA>2.0.CO;2.

Lu, R. Y., 2001: Interannual variability of the summertime North Pacific subtropical high and its relation to atmospheric convection over the warm pool. *J. Meteor. Soc. Japan*, **79**, 771–783, doi: 10.2151/jmsj.79.771.

Lu, R. Y., and B. W. Dong, 2001: Westward extension of North Pacific subtropical high in summer. *J. Meteor. Soc. Japan*, **79**, 1229–1241, doi: 10.2151/jmsj.79.1229.

Mao, J. Y., G. X. Wu, and Y. M. Liu, 2003: Study on the variation in the configuration of subtropical anticyclone and its mechanism during seasonal transition. Part I: Climatological features of subtropical high structure. *Acta Meteor. Sinica*, **17**, 274–286.

Mao, J. Y., Z. Sun, and G. X. Wu, 2010: 20–50-day oscillation of summer Yangtze rainfall in response to intraseasonal variations in the subtropical high over the western North Pacific and South China Sea. *Climate Dyn.*, **34**, 747–761, doi: 10.1007/s00382-009-0628-2.

North, G. R., T. L. Bell, R. F. Cahalan, et al., 1982: Sampling errors in the estimation of empirical orthogonal functions. *Mon. Wea. Rev.*, **110**, 699–706, doi: 10.1175/1520-0493(1982)110<0699:SEITEO>2.0.CO;2.

Qian, W. H., and J. Shi, 2017: Tripole precipitation pattern and SST variations linked with extreme zonal activities of the western Pacific subtropical high. *Int. J. Climatol.*, **37**, 3018–3035, doi: 10.1002/joc.4897.

Ren, R. C., Y. M. Liu, and G. X. Wu, 2007: Impact of South Asian high on the short-term variation of the subtropical anticyclone over western Pacific in July 1998. *Acta Meteor. Sinica*, **65**, 183–197, doi: 10.11676/qxxb2007.018. (in Chinese)

Ren, X. J., X. Q. Yang, and X. G. Sun, 2013: Zonal oscillation of western Pacific subtropical high and subseasonal SST variations during Yangtze persistent heavy rainfall events. *J. Climate*, **26**, 8929–8946, doi: 10.1175/JCLI-D-12-00861.1.

Ren, X. J., D. J. Yang, and X. Q. Yang, 2015: Characteristics and mechanisms of the subseasonal eastward extension of the South Asian high. *J. Climate*, **28**, 6799–6822, doi: 10.1175/JCLI-D-14-00682.1.

Tao, S. Y., and F. K. Zhu, 1964: The 100-hPa flow patterns in southern Asia in summer and its relation to the advance and retreat of the West Pacific subtropical anticyclone over the Far East. *Acta Meteor. Sinica*, **34**, 387–396, doi: 10.11676/qxxb1964.039. (in Chinese)

Tao, S. Y., and L. X. Chen, 1987: A review of recent research on the East Asian summer monsoon in China. *Monsoon Meteorology*, C. P. Chang, and T. N. Krishnamurti, Eds., Oxford University Press, New York, 60–92.

Wang, L. J., X. Chen, Z. Y. Guan, et al., 2009: Features of the short-term position variation of the western Pacific subtropical high during the torrential rain causing severe floods in southern China and its possible cause. *Chinese J. Atmos. Sci.*,

33, 1047–1057, doi: 10.3878/j.issn.1006-9895.2009.05.15. (in Chinese)

Wang, L. J., H. Gao, Z. Y. Guan, et al., 2011: Relationship between the western Pacific subtropical high and the subtropical East Asian diabatic heating during South China heavy rains in June 2005. *Acta Meteor. Sinica*, **25**, 203–210, doi: 10.1007/s13351-011-0027-6.

Wen, M., J. H. He, and Y. K. Tan, 2003: Movement of the ridge line of summer West Pacific subtropical high and its possible mechanism. *Acta Meteor. Sinica*, **17**, 37–51.

Wen, M., and X. H. Shi, 2006: Relationship between activity of West Pacific subtropical high and condensation latent heating in summer of 1998. *Plateau Meteor.*, **25**, 616–623, doi: 10.3321/j.issn:1000-0534.2006.04.008. (in Chinese)

Wu, G. X., Y. M. Liu, and P. Liu, 1999: The effect of spatially nonuniform heating on the formation and variation of subtropical high. I: Scale analysis. *Acta Meteor. Sinica*, **57**, 257–263, doi: 10.11676/qxxb1999.025. (in Chinese)

Yanai, M., and T. Tomita, 1998: Seasonal and interannual variability of atmospheric heat sources and moisture sinks as determined from NCEP–NCAR reanalysis. *J. Climate*, **11**, 463–482, doi: 10.1175/1520-0442(1998)011<0463:SAIVOA>2.0.CO;2.

Yanai, M., S. Esbensen, and J. H. Chu, 1973: Determination of bulk properties of tropical cloud clusters from large-scale heat and moisture budgets. *J. Atmos. Sci.*, **30**, 611–627, doi: 10.1175/1520-0469(1973)030<0611:DOBPOT>2.0.CO;2.

Yang, J., B. Wang, B. Wang, et al., 2010: Biweekly and 21–30-day variations of the subtropical summer monsoon rainfall over the lower reach of the Yangtze River basin. *J. Climate*, **23**, 1146–1159, doi: 10.1175/2009JCLI3005.1.

Yang, J., Q. Bao, B. Wang, et al., 2014: Distinct quasi-biweekly features of the subtropical East Asian monsoon during early and late summers. *Climate Dyn.*, **42**, 1469–1486, doi: 10.1007/s00382-013-1728-6.

Zhang, C. D., and J. Ling, 2012: Potential vorticity of the Madden–Julian Oscillation. *J. Atmos. Sci.*, **69**, 65–78, doi: 10.1175/JAS-D-11-081.1.

Zhang, R., and S. H. Yu, 1992: On the dynamic mechanism of biweekly oscillation of subtropical high over the western Pacific in summer. *J. Trop. Meteor.*, **8**, 306–314, doi: 10.16032/j.issn.1004-4965.1992.04.003. (in Chinese)

Zhou, T. J., R. C. Yu, J. Zhang, et al., 2009: Why the western Pacific subtropical high has extended westward since the late 1970s? *J. Climate*, **22**, 2199–2215, doi: 10.1175/2008JCLI2527.1.

Tech & Copy Editor: Lan YI